System-by-Design Paradigm-Based Synthesis of Complex Systems - The Case of Spline-Contoured 3D Radomes

M. Salucci, *Member, IEEE*, G. Oliveri, *Senior Member, IEEE*, M. A. Hannan, and A. Massa, *Fellow, IEEE*

***Abstract*—A macro-level overview of the System-by-Design (*SbD*) paradigm is illustrated and then applied to the design of a representative complex system. By introducing a set of archetypes of the *SbD* Paradigm (i.e., *Architecture-by-Design*, *Material-by-Design*, *Algorithm-by-Design*, and *Component-by-Design*), the synthesis of large complex-shaped radomes is addressed by combining the *Material-by-Design* and the *Architecture-by-Design* concepts. The results of a numerical assessment are discussed to give the interested readers some insights on the *SbD* effectiveness and potentialities also in comparison with traditional design approaches.**

***Index Terms*—System-by-Design (*SbD*), Complex Systems, Radomes, Radar Antennas, Metamaterials, Task-oriented Materials, Wide-Angle Impedance Matching (*WAIM*) layers.**

I. Introduction and Motivation

THE EFFICIENT and effective design of complex systems comprising several interconnected sub-parts is a challenging task that arises in several applicative domains belonging to the Antennas and Propagation field (e.g., radars, medical and industrial imaging, wireless communications, microwave devices, remote sensing) and, more in general, to the Engineering framework [1]-[2]. With reference to the Electromagnetics literature, several approaches have been proposed to handle the synthesis of complex systems. “Trial-and-error” or “parametric analysis” procedures were the firstly and widely adopted strategies thanks to their algorithmic simplicity and computational efficiency [3][4]. In these approaches, each component of the overall system undergoes an independent design process where the geometrical/electromagnetic descriptors or design variables (i.e., the size, the shape, and the electromagnetic properties of the materials) are varied within a predefined range [3][4] and a set of parametric curves are (numerically and/or experimentally) derived [3][4]. The designer is then asked to set the optimal values of the descriptors to fit the user-defined figures of merit on each sub-part of the system at hand. Unfortunately, such an approach cannot be employed when there are several and inter-dependent parameters to be modified because of the very large (and practically unfeasible) number of parametric evaluations to be carried out.

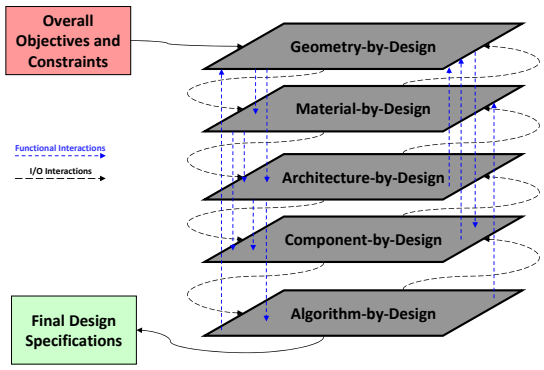

Figure 1. *SbD Paradigm* - Archetypes of the *SbD* paradigm with functional and input/output interconnections.

To partially overcome such an issue, local/global optimization methodologies [5]-[7] have been exploited for the independent design of each system component [8]. More in detail, the matching of the design requirements is yielded by an efficient iterative optimization (analytic [9], deterministic, or stochastic [8]) of the geometrical and/or electromagnetic (*EM*) descriptive parameters [namely, the degrees-of-freedom (*DoF*s)] of each sub-system [8], which are are combined in the overall architecture. A typical implementation of this guideline is the synthesis of large phased arrays based on the independent design of the radiating element [10], of the array architecture [9], of the feed network, and of the radome [8][11]. Such a methodology has several pros in terms of numerical efficiency (e.g., a parametric study for each design variable is not required) and modularity, but it neglects the physical relationships between the components of a complex system as profitably done by cross-layer or *holistic* approaches. These latter have recently emerged to deal with the design and the control of complex systems operating in highly dynamic scenarios [12]. In such a case, the design

Manuscript received Month DD, YYYY

The authors are with are with the ELEDIA@UniTN (University of Trento), Via Mesiano 77, 38123 Trento - Italy (e-mail: {marco.salucci, giacomo.oliveri, mohammadabdul.hannan, andrea.massa}@unitn.it)

A. Massa is also with the ELEDIA Research Center (ELEDIA@UESTC - UESTC), School of Electronic Engineering, Chengdu 611731 - China (e-mail: andrea.massa@uestc.edu.cn)

A. Massa is also with the ELEDIA Research Center (ELEDIA@TSINGHUA - Tsinghua University), 30 Shuangqing Rd, 100084 Haidian, Beijing - China (e-mail: andrea.massa@tsinghua.edu.cn)

This work benefited from the networking activities within the MIUR Project "CYBERPHYSICAL EM VISION" (grant 2017HZJXSZ)âPRIN2017 Program (CUP: E64I19002530001), the MIUR Project "MANTLES" (grant 2017BHFZKH) - PRIN2017 Program (CUP: E64I19000560001), the MIUR Project "WATERTECH" (grant SCN00489) - Program "Smart Cities and Communities and Social Innovation" (CUP: E44G14000060008), the MIUR Project "SMARTOUR - Piattaforma Intelligente per il Turismo" (grant SCN00166) - Program âSmart Cities and Communities and Social Innovation," and the Project "SPEED" (Grant No. 6721001) funded by the National Natural Science Foundation of China within the Changjiang Professorship program.

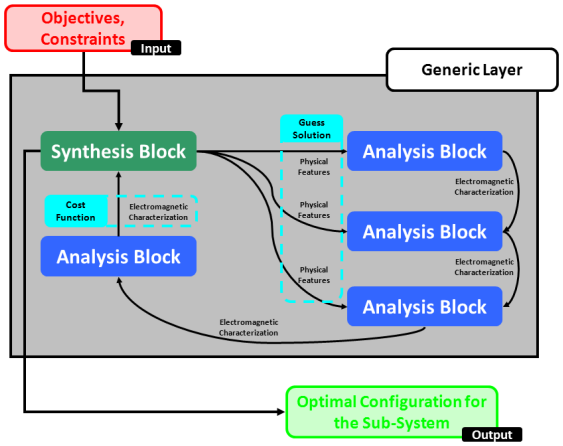

Figure 2. *SbD Paradigm* - Generic synthesis loop adopted in an *SbD* layer.

of the different "layers" of the system (from low-level HW to high-level communication and data fusion algorithms) is performed simultaneously [12] with an adaptive balance of the top-down demands and the bottom-up resource availability by creating bidirectional information flows across multiple layers of the system [12]. Unfortunately, *holistic* approaches are highly customized to address specific applicative scenarios (e.g., the design of *body sensor networks* [12] through *layers* exploiting high-level information on the "context" and low-level communication data), hence their generalization to a wider set of problems is generally prevented.

A different perspective for the synthesis of complex *EM* systems can be conceived starting from the observation that the design process is often representable as the *interconnection* of one or more designs of "blocks/functionalities" (Fig. 1). In complex *EM* problems [13]-[16], they include the *full-wave forward solver* block, the *homogenization* block, the *optimization / solution space exploration* block, the *tolerance error evaluation* block, the *material transformation* block, and the *real-time control* block. Such a perspective suggests to take into account, in the synthesis procedure, the relationships among the functional blocks so that each of them turns out to be an *enabling tool* for the methodology selection (i.e., to allow the choice of different "blocks" to meet the overall requirements, rather than focusing only on each specific task). For instance, the use of a fast *"full-wave-solver" block* for the element characterization is mandatory whether the associated *"optimization" block* requires several evaluations of the cost or objective function, while a slower solver is enough if the optimizer converges quickly. This concept is the core of the *System-by-Design* (*SbD*) paradigm, which can be defined as [13]-[16] "*a functional ecosystem to handle complexity in the design of large complex systems*."

The aim of this work is to give a macro-level overview of such a paradigm for the design of complex systems in which each functional block of the overall design procedure looks like an "enabler" for the choice of the other blocks to fit user-defined requirements under physical-admissibility design and consistency constraints. The relevance of this paradigm is demonstrated by the converging interdisciplinary research efforts on the use of numerical optimization for the design of complex systems, including the broad field of Multidisciplinary Design Optimization (*MDO*) [17]. To clarify the *SbD* concept and its features, a set of archetypes of the *SbD* Paradigm will be presented and various instances of the same *SbD* paradigm in various applicative scenarios will be illustrated including the *Architecture-by-Design*, the *Material-by-Design*, the *Algorithm-by-Design*, and *Component-by-Design* (Fig. 1). To illustrate and to assess the proposed paradigm, an applicative example concerned with the synthesis of a large complex-shaped radome will be carried out by combining the *Material-by-Design* and the *Architecture-by-Design* concepts. Towards this end, the radome design problem will be formulated in the *SbD* framework by defining a set of interconnected functional blocks. Afterwards, the arising solution method will be numerically validated also in comparison with recent state-of-the-art results. The paper is organized as follows. In Sect. II, the *SbD* Paradigm is firstly introduced and the fundamental classes of functional blocks of interest for complex *EM* designs are presented. Then, the *SbD*-based design of a radome (Sect. III) is detailed and numerically validated (Sect. IV). Finally, some conclusions and remarks are drawn (Sect. V).

II. System-by-Design Paradigm

A. SbD *Paradigm - Layered Interconnected Architecture*

According to the *SbD* paradigm [13]-[16], each "layer" of the design procedure of a generic complex system can be logically represented with a flowchart whose functional blocks are univocally identified by a set of inputs (constraints, objectives, and *DoF*s of all the sub-parts of the systems) and a set of outputs (design specifications and desired *EM* properties) (Fig. 2). Such functional blocks can be roughly subdivided into two categories (Fig. 2):

- *Analysis blocks* (blue boxes in Fig. 2) that receive the physical features of a device/sub-system to be analyzed (*input*) and return its *EM* response (e.g., radiated field/power pattern, *S* parameters, etc ...) (*output*);
- *Synthesis/Optimization blocks* (dark green boxes in Fig. 2) that generate the guess configurations for a device/sub-system (*output*) from the problem constraints and the associated cost function (*input*).

Since a complex design problem generally deals with multiple logical layers (e.g., architecture, algorithms, materials), a *SbD* process can be represented with a *multi-layer* scheme where each sub-part of the overall synthesis procedure is addressed in a different hierarchical level (Fig. 1), each *layer* being connected to the other ones through a set of functional and logical links and associated coupling variables (Fig. 1). Such a representation in terms of a set of interconnected loops (Fig. 1) allows one to (*i*) easily identify the functional blocks in the synthesis process so that "shared solutions" among different synthesis sub-problems are evident, (*ii*) understand admissible and different constraints/performance trade-offs among the *SbD* blocks. According to this view, the following main *SbD layers* can be defined (Fig. 1): (*a*) the "*Geometry-by-Design*"

layer, which consists of functional blocks devoted to the analysis/synthesis of the physical sizes/dimensions of the target subsystems (e.g., length of the devices, section, relevant geometrical descriptors); (*b*) the "*Material-by-Design*" layer related to the analysis/synthesis of task-oriented materials with desired *EM* properties (e.g., periodic or aperiodic lattices of elementary metallic and dielectric scatterers); (*c*) the "*Architecture-by-Design*" layer aimed at analyzing/synthesizing the layout of the sub-system (e.g., choice between different feeding network layouts, waveguide sections, antenna shapes, etc ...); (*d*) the "*Component-by-Design*" layer concerned with the optimal sub-components of the complex system (e.g., power dividers, phase shifters, amplifiers); (*e*) the "*Algorithm-by-Design*" dealing with the overall control strategies (e.g., the methodologies for the real-time array control).

B. SbD *Paradigm - Functional Blocks*

In the following, the *SbD* functional blocks for a generic *layer* (Fig. 1) of the design process are described. As for the **forward solver block** (*analysis*), a very large number of modelling techniques has been developed for the numerical solution of Maxwell's equations [18] to describe all the *EM* interactions of the complex system at hand. However, such methods may not be suitable for an efficient integration in complex synthesis schemes (Fig. 2) because of their unavoidable computational complexity [16]. A set of alternative strategies consists of "ad-hoc" numerical approaches that, instead of directly solving Maxwell's equations, exploit the knowledge of some features of the solution to considerably enhance the computational efficiency [14][15] of the arising *EM* analysis tool. Unfortunately, their application is intrinsically limited to "canonical" structures. A more recently investigated possibility is the use of *emulators* aimed at building, by means of ad-hoc *learning-by-example* (*LBE*) strategies [16][19][20], suitable *Surrogate Models* that efficiently "mimic" the *EM* full-wave solvers. Starting from a set of input-output examples, which are built with full-wave simulators and/or measurements, a prediction approach is trained to emulate the direct solver. When an additional information on the prediction accuracy is available [16][19][20], the *surrogate model* can be dynamically updated whenever the estimated accuracy falls below a threshold [19][20][16]. Despite several and considerable advantages, it is worth pointing out that some challenges have still to be addressed, including the *curse of dimensionality*, to fully and profitably exploit *LBE* methods within the "forward solver block".

Different procedures can be adopted for implementing the **homogenization block** (*analysis*) depending on what features of the inhomogeneous material must be replicated by the equivalent model, while taking into account the expected computational complexity and accuracy [21], as well. The "equivalence" is usually (*i*) an *external equivalence* (i.e., matching the scattering and transmission matrices as a function of the frequency and the wavenumber) or (*ii*) a *dispersion equivalence* (i.e., same solutions for the dispersion equation for the dominant eigenmodes) or (*iii*) a *single-mode equivalence* (i.e., matching the field distribution supported by a single eigenmode) or (*iv*) a *full-modal equivalence* (i.e., matching the field distributions supported by all the eigenmodes within the media) [21].

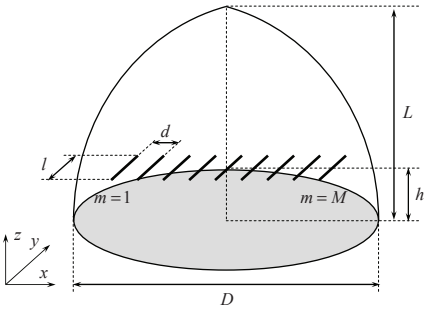

Figure 3. SbD *at work* - Geometry of the antenna-radome system.

As far as the **solution-space-exploration block** (*synthesis*) is concerned, the available algorithms can be classified either as deterministic or as stochastic [5]-[7]. Both are based on iterative search procedures devoted to generate a sequence of guess solutions converging to the global optimum of the cost function, which mathematically codes the user-requirements and physical constraints, to be optimized (minimized or maximized). More specifically, a new solution $\mathbf{f}_{i+1}$ is generated, starting from the current one $\mathbf{f}_i$, as follows

$$\mathbf{f}_{i+1} = \mathbf{f}_i + \Delta\mathbf{f}_i \tag{1}$$

where $\Delta\mathbf{f}_i$ is the update step at the i-th ($i = 1, ..., I$) iteration that, in principle, can be computed through local/deterministic or global/stochastic approaches [6]. In particular, (*i*) *Local Techniques* define the update step as $\Delta\mathbf{f}_i = \alpha_i\mathbf{d}_i$, where α_i is the step length and $\mathbf{d}_i$ is the search direction, both deterministically computed; (*ii*) *Global Techniques* feature stochastic operators to compute $\Delta\mathbf{f}_i$ [6] by processing single (*Single-Agent Methods*) or multiple (*Multiple-Agents Methods*) guess solutions at each i-th ($i = 1, ..., I$) iteration [5]-[7].

Whenever the fabrication tolerances must be taken into account in the synthesis process [22], the **tolerance error evaluation block** (*analysis*) is present to compute the performance "bounds" of a given sub-system from its physical features and expected fabrication errors. Towards this end, the commonly adopted approaches are (*i*) the Monte Carlo-like techniques [23] simple to implement, but not inclusive owing to their intrinsic statistical nature [22] and (*ii*) *Interval Analysis* methods, recently investigated within the *EM* framework [22], that allow the designer to analytically compute closed-form and inclusive performance bounds [22].

The aim of the **material transformation block** (*synthesis*), which is a distinctive element of the *Material-by-Design* layer, is the computation of the *EM* properties of a sub-device when a geometrical transformation (e.g., stretching and/or compression) is applied [24]. This functional block is fundamental whenever the synthesis of an unknown artificial material is formulated as the geometrical transformation of a known one as in several "lens" design problems [24]. Different *Transformation Electromagnetic* [24][25] or *Field Transformation* techniques [26] are usually considered to implement

such a functional block in the *SbD* paradigm depending on the applicative scenario at hand.

Finally, the **real-time control block** (*synthesis*) is present in several *EM* design problems [27] when dealing with the *Algorithm-by-Design* layer. In order to determine the optimal configuration for the control parameters of a dynamic system, given the real-time observed system performance [27], the problem is formulated as the optimization of a suitable cost function and a subset of the techniques used in the "solution-space exploration block" can be adopted. On the other hand, it is worthwhile pointing out that *ad-hoc* strategies based on the physics of the problem at hand (e.g., including memory-driven operators) turn out to be often more appropriate [27].

III. *SbD* Customization to *3D* Radome Design

A. Problem Statement

To illustrate an application of the *SbD* paradigm to a practical design example, the synthesis of a large three-dimensional variable thickness ogive radome [28][29] covering a phased array antenna is discussed hereinafter (Fig. 3). The choice of such a benchmark problem has the following motivations: (*i*) radome technology is of fundamental importance in several sensing and communication scenarios; (*ii*) the material of a radome and its internal structure play a key role in minimizing the performance distortions caused by attenuation, scattering, and de-polarization effects [30] especially when *variable-thickness designs* [28][29] are of interest owing to the need to mitigate for the possible "lensing" effects [28][29]; (*iii*) despite the development of accurate radome analysis/design methods [31], the integration of full-wave simulations within the design process is affordable only in a "local" refinement phase, while a global optimization is feasible only using simplified transmission-line models that provide approximate *EM* predictions [32]; (*iv*) *SbD* appears to be a natural choice to deal with the high computational complexity associated to the problem at hand. Such a complexity is actually caused by the multi-scale nature of the benchmark problem (e.g., micro-scale radome contouring variations vs. macro-scale propagation/distortion effects), by the need to accurately compute the near-field interactions among the antennas and between the radome and the array (requiring careful full-wave modeling of the entire structure), and by the large computational complexity of the associated EM model. More in detail, the radome is supposed to cover a linear phased array consisting of M dipoles of length l and inter-element spacing d located at a distance h over the ground plane (Fig. 3). It is characterized by an ogival shape with a circular basis on the xy-plane of diameter D and length L along the z-axis. Moreover, it is made of an homogeneous dielectric material with permittivity ε_r and loss tangent $tan\delta$, while its external curvature is given by the following equation

$$x^2 + y^2 = \left(\frac{D}{2L}\right)^2 \left(L^\xi - z^\xi\right)^{2/\xi} \tag{2}$$

where $z \in [0 : L]$ and ξ is a parameter associated to the curvature of the radome [33][(1)]. The synthesis problem at hand can be then stated as follows

> *Radome Design Problem* - Given ε_r, $tan\delta$, D, L, and ξ (user-defined descriptors) and the specifications of the array antenna, synthesize the internal profile of the radome, which is coded into the *DoF* vector $\mathbf{f}$, to minimize the boresight steering error (*BSE*) in the user-defined frequency, $\upsilon \in [\upsilon_{min}, \upsilon_{max}]$, and angular, $\theta \in [-\theta^{\max}, \theta^{\max}]$ [deg], ranges.

where υ is the working frequency, $[\upsilon_{min}, \upsilon_{max}]$ being the operation bandwidth, and θ is the scan angle ranging within the field-of-view $[-\theta^{\max}, \theta^{\max}]$, while the phases of the array are assumed to be set to the optimal values determined at the central frequency υ_0 without the radome. It is worth remarking that the co-design of the phased array, although potentially interesting, is not considered in the benchmark scenario owing to the practical and theoretical relevance of the problem of synthesizing an effective radome when the antenna array cannot be adjusted/modified [8][32]. Accordingly, the design constraints for the radome synthesis are collected in a vector $\mathcal{G} \triangleq \{g_c(\mathbf{f}); c = 1, ..., C\}$ comprising the radome material $g_{1,2}(\mathbf{f}) = \{\varepsilon_r, tan\delta\}$, its external shape $g_{3,4,5}(\mathbf{f}) = \{D, L, \xi\}$, the antenna parameters $g_{6,7,8,9}(\mathbf{f}) = \{M, l, d, h\}$, the working bandwidth $g_{10,11}(\mathbf{f}) = \{\upsilon_{min}, \upsilon_{max}\}$, and maximum steering angle $g_{12}(\mathbf{f}) = \{\theta^{max}\}$. To apply the *SbD* paradigm to such a "scenario", it is needed to specify (*i*) the mathematical description of the solution and the associated *DoF*s, (*ii*) the cost function that quantifies the mismatch of the *EM* performance of trial solution with the user requirements, and (*iii*) the *SbD* layers to be considered and the implementation of the corresponding functional blocks (Fig. 1). To this end, it is worth mentioning that the solution to the *Radome Design Problem* may not be unique owing to the *inverse* nature of the adopted formulation and the associated ill-posedness [6]. Nevertheless, and unlike inverse scattering [6], such a feature is actually an advantage in the addressed benchmark scenario since it potentially enables to select the most proper among the equivalent designs in terms of user-defined priorities (e.g., fabrication costs).

B. Solution Model Selection and DoFs Identification

To describe the radome solution model and to define the associated *DoF*s, let us observe that the axial symmetry of the structure (Fig. 3) allows one to describe the 3D dielectric structure in terms of the associated xz-plane section $\Gamma(x, z)$. Accordingly, a 2D basis set $\{B_n(x, z); n = 1, ..., N\}$ is used to encode the radome shape. While a pixel-basis model [Fig. 4(*a*)] could be employed to express $\Gamma(x, z)$

$$\Gamma^{(pix)}(x, z) = \sum_{n=1}^{N} f_n^{(pix)} B_n^{(pix)}(x, z) \tag{3}$$

being $B_n^{(pix)}(x, z) = 1$ if $(x, z) \in \Omega_n$ ($B_n^{(pix)}(x, z) = 0$ if $(x, z) \notin \Omega_n$) the n-th ($n = 1, ..., N$) basis function,

(1)The optimization of the external radome profile descriptors (material, D, L, and ξ) is beyond the scope of the current work since it would require a multi-physics modeling to account for mechanical / aerodynamic performance.

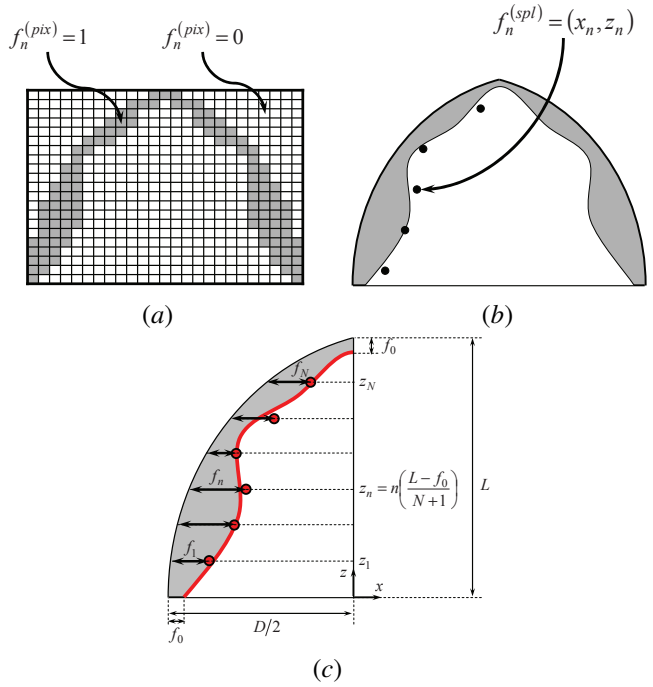

Figure 4. *Problem Formulation - Solution Model Selection* - Sketch of the (*a*) pixel-based and (*b*) spline-based representation of a radome profile, and (*c*) identification of the design parameters according to spline representation (f_n, $n=1,...,N$).

Ω_n is the support of the n-th discretization cell, and the solution descriptors are the set of binary coefficients $\{f_n^{(pix)}; n=1,...,N\}$ [where $f_n^{(pix)}=1/0$ indicates a cell belonging or not to the radome - Fig. 4(*a*)], unfortunately such an approach requires a large number of descriptors for an accurate and flexible parametric model of the radome structure. To overcome such an issue, a spline-based representation of the radome contour is conceived [Fig. 4(*b*)]. As a matter of fact, by using the Bezier quadratic spline curves [Fig. 4(*b*)], the *DoF*s of the solution reduce to the control points of the spline curve, $\{f_n^{(spl)}=(x_n,z_n); n=1,...,N\}$ and the basis functions that describe the radome profile turn out to be the following second order polynomials

$$B_n^{(spl)}\left(x,z;\mathbf{f}^{(spl)},t\right)=\left(1-t^2\right)\left(\frac{f_n^{(spl)}+f_{n+1}^{(spl)}}{2}\right)+ +2t\left(1-t\right)f_n^{(spl)}+t^2\left(\frac{f_{n+1}^{(spl)}+f_{n+2}^{(spl)}}{2}\right) \quad (4)$$

($n=1,...,N$), where $f_{N+1}^{(spl)}=f_1^{(spl)}$, $f_{N+2}^{(spl)}=f_2^{(spl)}$, and $t\in[0:1]$. Accordingly, the radome section is modeled as follows

$$\Gamma^{(spl)}(x,z)=\sum_{n=1}^{N}B_n^{(spl)}\left(x,z;\mathbf{f}^{(spl)},t\right) \quad (5)$$

to (*i*) minimize the number of descriptors, while (*ii*) efficiently and flexibly describing complex continuous radome contours. Therefore, $\mathbf{f}=\mathbf{f}^{(spl)}$ hereinafter under the condition that $z_n=n\left(\frac{L-f_0}{N+1}\right)$, $n=1,...,N$ [Fig. 4(*c*)]. Moreover, for the sake of simplicity, the thickness of the radome at the base and at the top of the profile is supposed to be equal to f_0 [Fig. 4(*c*)].

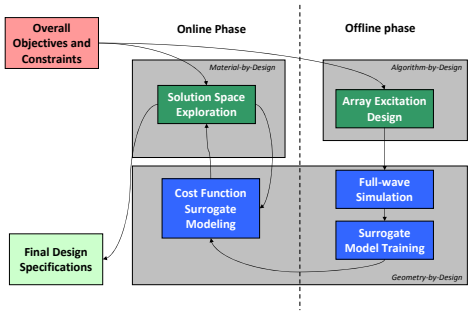

Figure 5. *Customized SbD Approach* - Functional scheme of the proposed radome design methodology.

C. Cost Function Definition

The cost function $\Phi(\mathbf{f})$ is the unique link between the design process and the physics of the problem at hand [6]. To mathematically encode the target of the "*Radome Design Problem*" (i.e., the *BSE* minimization), $\Phi(\mathbf{f})$ is defined as

$$\Phi(\mathbf{f})=\frac{\sum_{p=1}^{Q_\lambda}\sum_{q=1}^{Q_\theta}\left[\widehat{\theta}^{NO-RAD}(\theta_q,\lambda_p)-\widehat{\theta}^{RAD}(\theta_q,\lambda_p;\mathbf{f})\right]^2}{Q_\lambda\times Q_\theta} \quad (6)$$

where Q_λ is the number of radome working frequencies, λ_p being the corresponding p-th ($p=1,...,Q_\lambda$) wavelength, and Q_θ is the number of beam pointing directions, $\{\theta_q; q=1,...,Q_\theta\}$. In (6), the term $\widehat{\theta}^{NO-RAD}(\theta_q,\lambda_p)$ is the actual beam pointing direction of the antenna without the radome when setting the excitations of the array elements to steer the mainlobe peak of the power pattern, $P_{qp}^{NO-RAD}(\theta)$, along the q-th pointing direction at the p-th operation frequency

$$\widehat{\theta}^{NO-RAD}(\theta_q,\lambda_p)=arg\left\{\max_{\theta\in[0:90]\,[deg]}\left[P_{qp}^{NO-RAD}(\theta)\right]\right\}. \quad (7)$$

Moreover, $\widehat{\theta}^{RAD}(\theta_q,\lambda_p;\mathbf{f})$ is the actual pointing direction of the antenna with the radome, which is described by the set $\mathbf{f}$ of descriptors, while setting the element excitations as in (7)

$$\widehat{\theta}^{RAD}(\theta_q,\lambda_p;\mathbf{f})=arg\left\{\max_{\theta\in[0:90]\,[deg]}\left[P_{qp}^{RAD}(\theta;\mathbf{f})\right]\right\}. \quad (8)$$

D. SbD Layers and Loop Implementation

Once the problem has been formulated (Sect. III-A), the *DoF* have been selected (Sect. III-B), and the cost function has been defined (Sect. III-C), the functional scheme of the *SbD* paradigm for the synthesis problem at hand is derived (Fig. 5). In this case, the radome-oriented instance of the *SbD* paradigm must include the *Geometry-by-Design*, the *Material-by-Design*, and the *Algorithm-by-Design* layers (Fig. 5). Such layers need the following functional blocks (Fig. 5): (*i*) a cost function evaluation meta-block (Sect. III-D1) for the efficient evaluation of (6) yielded with a forward solver block featuring surrogate modeling along with a full-wave 3D simulation block, (*ii*) a solution-space exploration block (Sect. III-D2) to sample the solution space of the *DoF*s, and (*iii*) a real-time excitation design block for the control of the array boresight direction (not discussed in the following as it is based on a standard formulation [1]).

1) Cost Function Evaluation Meta-Block: The cost-function evaluation meta-block (6) for the radome design is implemented with a *LBE*-based surrogate model starting from S known input-output pairs $\{\mathbf{f}_s, \Phi(\mathbf{f}_s)\}$, $s = 1, ..., S$ (i.e., the *training set*) where the values $\{\Phi(\mathbf{f}_s);\ s = 1, ..., S\}$ are the results of S full-wave simulations (6)[(2)]. The choice of the training samples is a critical step to guarantee the required prediction accuracy without recurring to very large S. Towards this end, the Latin Hypercube Sampling (*LHS*) technique [16][20] is adopted since (*i*) it is possible to set the amount of time for the definition of the training set, S being *a-priori* chosen; (*ii*) the S training samples are uniformly distributed within the solution space, which is preferable when no *a-priori* info or test can be performed on the "relevance" of each feature. More in detail, the *LHS* process can be summarized into the following steps:

- **Step 1 - *Initialization***. Define the admissible range $\left[f_n^{\min}, f_n^{\max}\right]$, $n = 1, ..., N$, of each solution descriptor (i.e., *DoF*);
- **Step 2 - *Solution Space Segmentation***. Uniformly divide the range of variation of each n-th ($n = 1, ..., N$) *DoF* (i.e., $\Delta_n^{(s)} = [(s-1) \times \delta_n : s \times \delta_n]$, $s = 1, ..., S$, being $\delta_n \triangleq \frac{f_n^{\max} - f_n^{\min}}{S}$);
- **Step 3 - *Single Feature Sampling.*** For each n-th ($n = 1, ..., N$) *DoF,* f_n, randomly select S values, $\{f_{n,s};\ s = 1, ..., S\}$, one for each segment $\Delta_n^{(s)}$ (i.e., $f_{n,s} \in \Delta_n^{(s)}$, $s = 1, ..., S$);
- **Step 4 - *Training Sample Generation***. Generate a training sample $\mathbf{f}_s$ by uniformly picking, for each n-th ($n = 1, ..., N$) solution parameter, f_n, one of the S values $\{f_{n,s};\ s = 1, ..., S\}$. The s-th training sample is thus given by

$$\mathbf{f}_s = \{f_{n,j_s};\ n = 1, ..., N\} \tag{9}$$

  where $j_s \in [1 : S]$ and $f_{n,j_s} \neq f_{o,j_s}$, $n \neq o$, to select the value $f_{n,s}$ ($n = 1, ..., N$; $s = 1, ..., S$) only once.

Once the training set has been built, the Ordinary Kriging (*OK*) is adopted as *LBE* strategy in the *SbD* loop (Fig. 5). The main motivations of such a choice are that, unlike other *LBE* methods, the *OK* is very effective when high-fidelity input samples (i.e., not corrupted by noise as those coming from full-wave simulations) have to be processed since it guarantees that $\hat{\Phi}(\mathbf{f}_s) \equiv \Phi(\mathbf{f}_s)$, $s = 1, ..., S$. Moreover, it also provides an estimation of the prediction uncertainty, $\hat{\chi}(\mathbf{f}_n)$.
According to the *OK* strategy, the prediction for a generic descriptor setup $\mathbf{f}_i$ turns out to be

$$\hat{\Phi}(\mathbf{f}_i) \triangleq \hat{\mu} + \mathbf{r}^T(\mathbf{f}_i)\,\mathbf{R}^{-1}(\mathbf{\Phi} - \mathbf{I}\hat{\mu}) \tag{10}$$

where $\hat{\mu}$ is a constant term ($\hat{\mu} \triangleq \frac{\mathbf{I}^T\mathbf{R}^{-1}\mathbf{\Phi}}{\mathbf{I}^T\mathbf{R}^{-1}\mathbf{I}}$), $\mathbf{I}$ is an S-dimensional unitary vector $\mathbf{I} \triangleq [1, 1, ..., 1]^T$ (T denotes the transpose operation), $\mathbf{\Phi} = [\Phi(\mathbf{f}_1), ..., \Phi(\mathbf{f}_s), ..., \Phi(\mathbf{f}_S)]^T$, and $\mathbf{R}$ is the $S \times S$ correlation matrix whose j_s-th ($j_s = 1, ..., S$) entry is equal to

$$R_{j_s} = \prod_{n=1}^{N} \exp\left(-\alpha_n |f_{s,n} - f_{j,n}|^{\beta_n}\right), \tag{11}$$

$\boldsymbol{\alpha} = \{\alpha_n : n = 1, ..., N\}$ and $\boldsymbol{\beta} = \{\beta_n : n = 1, ..., N\}$ being two sets of control hyper-parameters. Moreover, $\mathbf{r}(\mathbf{f}_i)$ is a S-dimensional vector

$$r_s(\mathbf{f}_i) = \prod_{n=1}^{N} \exp\left(-\alpha_n |f_{s,n} - f_{i,n}|^{\beta_n}\right) \tag{12}$$

($s = 1, ..., S$). As it can be noticed (10), the prediction of the cost function value $\hat{\Phi}(\mathbf{f}_i)$ is proportional to the correlation/distance between the new trial solution $\mathbf{f}_i$ and the S training samples (12) and from the correlation between the training solutions (11) as well as their fitness values $\mathbf{\Phi}$. Concerning the optimal setup of the hyper-parameters in (11) and (12), it is yielded by maximizing the following *Likelihood Function*

$$\Xi(\boldsymbol{\alpha}, \boldsymbol{\beta}) = -\frac{S}{2} ln\left(\hat{\sigma}^2\right) - \frac{1}{2} ln\left|\mathbf{R}\right| \tag{13}$$

where $\hat{\sigma}^2 = \frac{(\mathbf{\Phi} - \mathbf{I}\hat{\mu})^T \mathbf{R}^{-1} (\mathbf{\Phi} - \mathbf{I}\hat{\mu})}{S}$, $|.|$ being the determinant operator. Finally, the prediction uncertainty, $\hat{\chi}(\mathbf{f}_i)$, is computed as

$$\hat{\chi}(\mathbf{f}_i) = \sqrt{\hat{\sigma}^2 \left[1 - \mathbf{r}^T(\mathbf{f}_i)\,\mathbf{R}^{-1}\mathbf{r}(\mathbf{f}_i) + \frac{\left(1 - \mathbf{I}\mathbf{R}^{-1}\mathbf{r}(\mathbf{f}_i)\right)^2}{\mathbf{I}\mathbf{R}^{-1}\mathbf{I}}\right]}, \tag{14}$$

to give an index of the self-detected surrogate model accuracy.

2) Solution Space Exploration Block: The "No Free-Lunch (*NFL*) Theorem" [13][34] states that (*i*) the application of an arbitrary optimization algorithm to a problem without taking care of the nature of the cost function and of the *DoF* features is on average equivalent to use a random search and that (*ii*) each optimization algorithm has its own "optimal niche" of application in which it outperforms other approaches. Following such guidelines and the state-of-the-art analysis [6], a Particle Swarm Optimization (*PSO*)-inspired approach has been employed in the following owing to the high non-linearity of the problem at hand (6) and the real-valued nature of the solution descriptors [i.e., the control points of the spline curve used to model the radome profile - Eq. (4)].

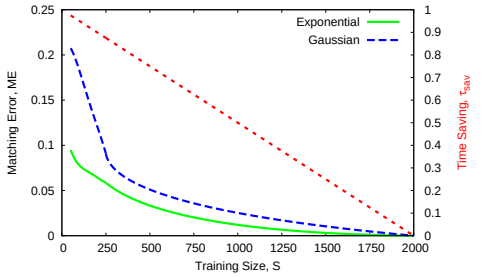

Figure 6. *Numerical Validation* ($S \in [50 : 2000]$) - Behaviour of ME and τ_{sav} versus S when considering the Gaussian ($\beta_n = 2$) and the exponential ($\beta_n = 1$) correlation models.

[(2)]The adopted *FEM*-based full-wave numerical modeling approach (i.e., *Ansys HFSS*) intrinsically accounts for the currents induced into the radome structure therefore allowing to evaluate the arising antenna pattern and directivity modifications.

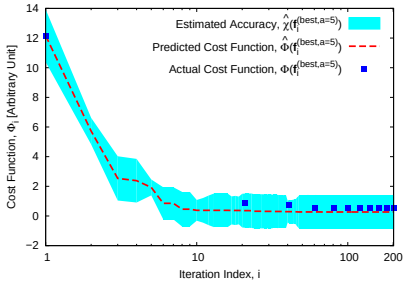

Figure 7. *Numerical Assessment* ($S = 250$) - Evolution of the predicted cost function value, $\hat{\Phi}\left(\mathbf{f}_i^*\right)$, of the corresponding estimation accuracy $\hat{\chi}\left(\mathbf{f}_i^*\right)$, and of the actual cost function values $\Phi\left(\mathbf{f}_i^*\right)$.

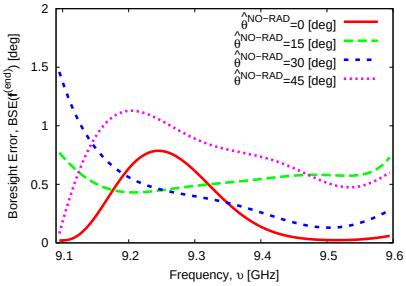

Figure 8. *Numerical Assessment* ($S = 250$, $a = 5$, $\mathbf{f} = \mathbf{f}^{(end)}$) - Behavior of the *BSE* versus υ.

IV. Numerical Assessment

An ogive radome with a circular base $D = 30.7\,\lambda_0$ in diameter and length $L = 17\,\lambda_0$ (λ_0 being the free-space wavelength at $\upsilon_0 = 9.345$ [GHz]) has been chosen as benchmark for the *SbD* assessment. With reference to Sect. III-A, the linear phased array consists of $M = 8$ parallel dipoles of length $l = \frac{\lambda_0}{2}$ and inter-element distance $d = \frac{\lambda_0}{2}$ working over a 500 [MHz] bandwidth from $\upsilon_{min} = 9.095$ [GHz] up to $\upsilon_{max} = 9.595$ [GHz][(3)]. It has been located at the center of the radome base at a height $h = \frac{\lambda_0}{4}$ from the ground plane (Fig. 3). The radome is composed of Teflon with $\varepsilon_r = 2.1$ and $\tan\delta = 3.0 \times 10^{-4}$ [30], while its external curvature (2) has been defined by choosing $\xi = 1.6$ and $f_0 = \frac{\lambda_0}{\sqrt{\varepsilon_r}2} = \frac{\lambda_r}{2}$. The maximum scan angle has been set at $\theta^{\max} = 45$ [deg][(4)]. According to the guidelines in [6], the solution space exploration block has been used with the following calibration setup: $G = 2 \times N$, inertial weight $w = 0.4$, cognitive and social acceleration coefficients $C_1 = 2.0$ and $C_2 = 2.0$, respectively, and $I_{SbD} = 200$ (G being the size of the *PSO* population and I_{SbD} being the maximum number of optimization iterations).

A. Cost Function Prediction Accuracy vs. Complexity

The first numerical experiments deals with the evaluation of the accuracy of the *Cost Function Evaluation* meta-block versus the size of the training set, S. Such an assessment is of fundamental importance to choose a suitable trade-off between prediction accuracy and computational saving for the problem at hand [16]. Towards this end, a set of experiments has been carried out by ranging S in $S \in \left[S^{\min}, S^{\max}\right] = [50, 2000]$, $S^{\max}$ being the maximum number of guess solutions generated throughout the optimization process until the convergence ($S^{\max} \triangleq G \times I_{SbD}$). Each S-sized training set has been *LHS*-defined by setting $f_n^{\min} = 0.2$ $[\lambda_r]$ and $f_n^{\max} = 0.8$ $[\lambda_r]$, $n = 1, ..., N$ [Fig. 4(*c*)], λ_r being the wavelength in the radome, and by choosing $N = 5$ spline control points. Moreover, each antenna-radome structure has been analyzed by considering $Q_\theta = 4$ and $Q_\lambda = 11$ samples uniformly distributed in the angular range and in the frequency one, respectively. Finally, $V = 100$ solutions, $\{\mathbf{f}_v;\ v = 1, ..., V\}$, not belonging to the training set ($\mathbf{f}_s \neq \mathbf{f}_v;\ s = 1, ..., S;\ v = 1, ..., V$) have been used for the validation set and the prediction accuracy has been evaluated in terms of the *matching error index* (ME)

$$ME = \frac{\sum_{v=1}^{V} \left|\hat{\Phi}\left(\mathbf{f}_v\right) - \Phi\left(\mathbf{f}_v\right)\right|^2}{\sum_{v=1}^{V} \left|\Phi\left(\mathbf{f}_v\right)\right|^2}. \tag{15}$$

where $\hat{\Phi}\left(\mathbf{f}_v\right)$ and $\Phi\left(\mathbf{f}_v\right)$ stand for the predicted and the actual value of the cost function, respectively. Figure 6 shows the behaviour of ME versus S when considering either the exponential ($\beta_n = 1$) or the Gaussian ($\beta_n = 2$) correlation model along with the corresponding time saving factor τ_{sav} ($\tau_{sav} \triangleq \frac{T_{Std} - T_{SbD}}{T_{Std}}$), T_{Std} and T_{SbD} being the *CPU*-time for predicting the V samples with the *OK*-based surrogate model (*SbD*) and with a conventional full-wave simulator, respectively. As it can be inferred (Fig. 6), it turns out that (*i*) there are different trade-offs depending on the available resources (S) and a desired emulation fidelity, (*ii*) the exponential correlation model always outperforms the Gaussian one in terms of accuracy (green vs. blue lines - Fig. 6), (*iii*) owing to the very large computational costs associated to the radome simulation, despite the relatively low value of Q_θ (i.e., $S^{\max}$ training samples would require > 12 years of computation on a single processor), a careful choice of the training set size, S, is mandatory to yield a feasible synthesis (i.e., computationally-admissible trade-off between accuracy and offline simulation effort). With reference to the choice of the training set size, the $S = 250$ setup has been chosen since it gives a good prediction accuracy (i.e., $ME|_{S=250} = 5.85\%$) with a non-negligible computational efficiency (i.e., $\tau_{sav}|_{S=250} \approx 87.5\%$). Moreover, such a value is compliant with the state-of-the-art guidelines regarding *LHS* initial training samples for five-dimensional problems (i.e., $N = 5$) as discussed in [35]. For the sake of completeness, Table I reports the statistics of the actual cost function value for the $S = 250$ training samples.

B. SbD-based Synthesis Results

The next numerical experiment is aimed at assessing the effectiveness of the *SbD*-based synthesis strategy from the performance and statistical viewpoint. Therefore, $A = 100$

[(3)]Owing to the base diameter and overall size of the benchmark radome, the derived conclusions are actually valid also for much larger array setups. Within this framework, no change is expected from the methodological viewpoint to the algorithm to handle arrays of different sizes.

[(4)]The full-wave simulation of a single radome requires ≈ 56 hours on a single-CPU desktop PC running at 3.6 [GHz] with 32 GB of RAM.

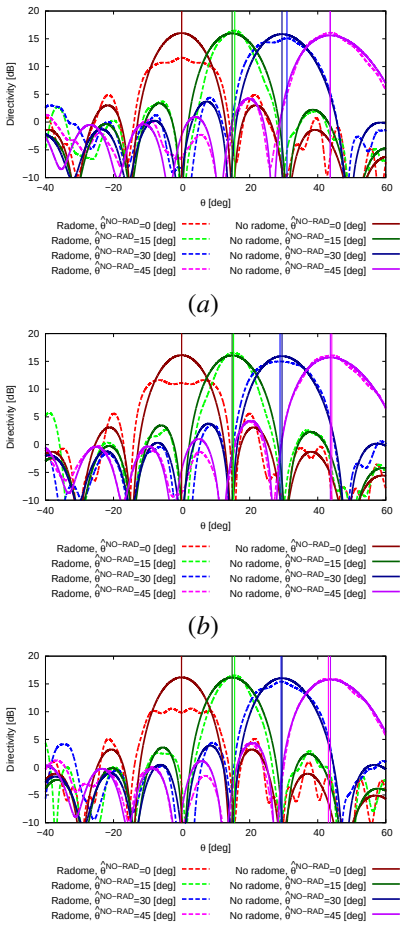

Figure 9. *Numerical Assessment* ($S = 250$, $\mathbf{f} = \mathbf{f}^*$) - Directivity patterns and pointing accuracy (vertical lines) with and without radome when (*a*) $\upsilon_{min} = 9.095$ [GHz], (*b*) $\upsilon_0 = 9.345$ [GHz], and (*c*) $\upsilon_{max} = 9.595$ [GHz].

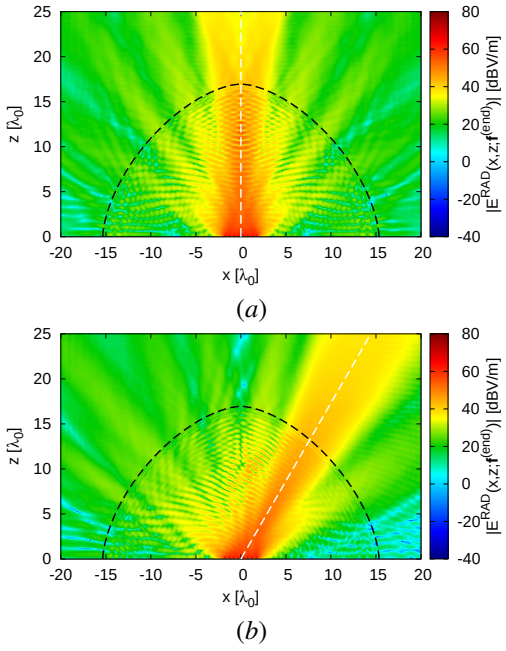

Figure 10. *Numerical Assessment* ($S = 250$, $\mathbf{f} = \mathbf{f}^*$) - Electric field magnitude with radome when (*a*) $\widehat{\theta}^{NO-RAD}(\theta_1, \lambda_0) = 0$ [deg] and (*b*) $\widehat{\theta}^{NO-RAD}(\theta_3, \lambda_0) = 30$ [deg].

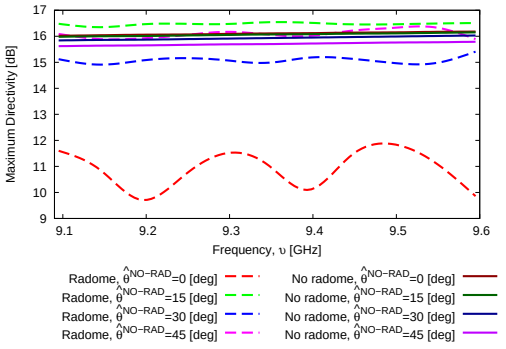

Figure 11. *Numerical Assessment* ($S = 250$, $\mathbf{f} = \mathbf{f}^*$) - Maximum directivity with and without radome versus frequency for different scan angles.

different simulations have been run starting from the same initial swarm, but using a different seed to generate different sequences of trial solutions throughout the optimization process. The statistics for the optimal prediction of the cost function value, $\hat{\Phi}\left(\mathbf{f}^{(a)}\right)$, $\mathbf{f}^{(a)}$ being the best design obtained at the convergence of the a-th ($a = 1, ..., A$) run (Tab. I) indicate that the optimization process is very stable since different simulations converge to very close design values.

The effectiveness of the *SbD* synthesis is discussed next by analyzing the best solution among the A runs. When analyzing the performance of the optimal *SbD* solution setup $\mathbf{f}^* = \{0.55, 0.69, 0.54, 0.73, 0.47\}$ with a full-wave solver, it turns out that (*i*) the actual value of the cost function, $\Phi(\mathbf{f}^*) = 0.55$, is smaller than the minimum of the training set [i.e., $\Phi^{(min)}(\mathbf{f}_s) = 0.89$ - Tab. *I*] and that (*ii*) the synthesized radome excellently performs (i.e., $ME < 1\%$). Moreover, the comparison of the behaviors of the actual and predicted optimal cost function values versus the iteration index points out an excellent agreement (Fig. 7) as well as the fact that the actual cost function values belong the "tube" of the estimated uncertainty, whose bounds are (14) $\hat{\Phi}(\mathbf{f}_i^a) \pm \hat{\chi}(\mathbf{f}_i^a)$, $i = 1, ..., I_{SbD}$.

The next set of numerical results is aimed at showing the performance of the *SbD*-designed radome. The frequency behaviour of the *BSE* when setting $\widehat{\theta}^{NO-RAD}(\theta_q, \lambda_0) = \{0, 15, 30, 45\}$ [deg] (Fig. 8) and the directivity patterns generated at the minimum frequency [$\upsilon_{min} = 9.095$ GHz - Fig. 9(*a*)], central frequency [$\upsilon_0 = 9.345$ GHz - Fig. 9(*b*)], and maximum frequency [$\upsilon_{max} = 9.595$ GHz - Fig. 9(*c*)] show that (*i*) highly directive and well-shaped beam patterns scanned along the desired directions are generally afforded (Fig. 8), (*ii*) the performance deterioration when scanning along broadside is caused by reflections of portion of the *EM* energy from the radome to the antenna [Fig. 10(*a*)] with a perturbation of the field $\underline{E}^{RAD}(x, z; \mathbf{f}^*)$ with respect to an off-broadside scan [Fig. 10(*b*)]; (*iii*) accordingly, limited directivity variations with pointing direction and frequency with/without the radome are observed (Fig. 11).

For the sake of completeness, the plots of the *S*-parameters of

Table I
Numerical Assessment ($S = 250$, $A = 100$) - STATISTICAL FEATURES OF TRAINING SET COST FUNCTION $\Phi(\mathbf{f}_s)$, $s = 1, ..., S$, AND OF PREDICTED COST FUNCTION AT THE CONVERGENCE OF OF EACH a-TH ($a = 1, ..., A$) TRIAL SIMULATION, $\hat{\Phi}\left(\mathbf{f}^{(a)}\right)$.

	$\Phi(\mathbf{f}_s)$	$\hat{\Phi}\left(\mathbf{f}^{(a)}\right)$
min	0.89	0.49
max	16.25	2.70
avg	5.23	1.15
std − dev	3.26	0.60

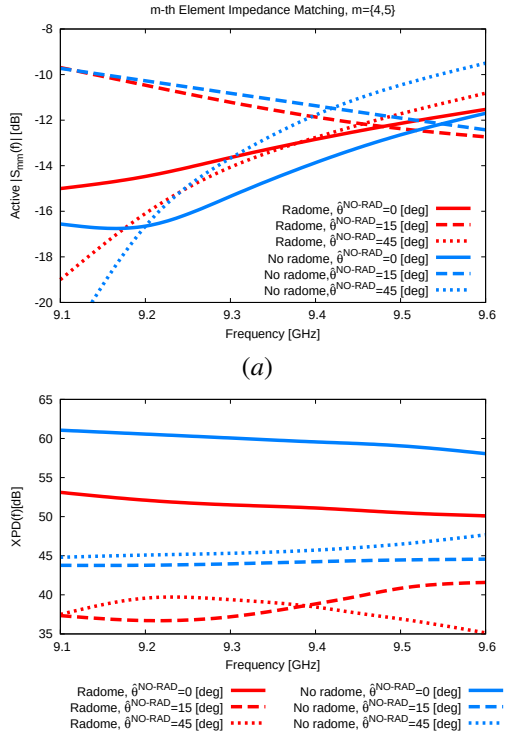

Figure 12. *Numerical Assessment* ($S = 250$, $\mathbf{f} = \mathbf{f}^*$) - Behaviour of (*a*) $m = \{4, 5\}$ array elements *S*-parameters and (*b*) cross-polar discrimination versus frequency when $\widehat{\theta}^{NO-RAD}(\theta_1, \lambda_0) \in \{0, 15, 45\}$ [deg].

the $m = \{4, 5\}$ array elements [Fig. 12(*a*)] and the ratio of the co-polar vs. cross-polar components [i.e., cross-polar discrimination (XPD) - Fig. 12(*b*)] with or without the radome assuming $\widehat{\theta}^{NO-RAD}(\theta_1, \lambda_0) \in \{0, 15, 45\}$ show that (*i*) even though such parameters are not addressed in the optimization problem, a satisfactory return loss is obtained in all cases [i.e., reflection below -9 dB in the entire band - Fig. 12(*a*)] even in worst-case conditions (i.e., $\widehat{\theta}^{NO-RAD}(\theta_1, \lambda_0) = 15$ [deg]) and despite the simple radiators at hand, and that (*ii*) the presence of the radome has a marginal effect on the polarization purity of the considered arrangement [i.e., $XPD^{NO-RAD} > 44$ dB vs. $XPD^{RAD} > 35$ dB - Fig. 12(*b*)].

The final set of experiments is devoted to the demonstration of the search capabilities of the proposed *SbD* paradigm when multiple design objectives are taken into account. Towards this end, the same benchmark setup has been dealt with, but attenuation and structural considerations have been included beyond boresight steering error. More in detail, (6) has been substituted with a extended cost function $\Phi^{MO}(\mathbf{f})$ defined as

$$\Phi^{MO}(\mathbf{f}) = \Phi(\mathbf{f}) + \Phi^{ATT}(\mathbf{f}) + \Phi^{WGT}(\mathbf{f}) \qquad (16)$$

where $\Phi^{ATT}(\mathbf{f}) = \frac{\sum_{p=1}^{Q_\lambda}\sum_{q=1}^{Q_\theta}\left[G_{\max}^{NO-RAD}(\theta_q,\lambda_p) - G_{\max}^{RAD}(\theta_q,\lambda_p;\mathbf{f})\right]}{Q_\lambda \times Q_\theta}$ accounts for the attenuation, $G_{\max}^{NO-RAD}(\theta_q, \lambda_p)/G_{\max}^{RAD}(\theta_q, \lambda_p)$ being the maximum gain (expressed in dB) when steering the beam towards the direction θ_q at frequency λ_p without/with the radome, respectively, and $\Phi^{WGT}(\mathbf{f}) \triangleq \frac{\Psi(\mathbf{f})}{\Psi(\mathbf{f}^{\min})}$ accounts for the radome structural properties, $\Psi(\cdot)$ being the radome weight, and $\mathbf{f}^{\min} \triangleq \left\{f_n^{\min};\, n = 1, ..., N\right\}$ the minimum-thickness radome setup. The evolution of $\hat{\Phi}^{MO}(\mathbf{f}_i^*)$, $\hat{\Phi}(\mathbf{f}_i^*)$, $\hat{\Phi}^{ATT}(\mathbf{f}_i^*)$, and $\hat{\Phi}^{WGT}(\mathbf{f}_i^*)$ versus the iteration number (Fig. 13) further demonstrates the *SbD* search capabilities in terms of boresight steering error reduction (i.e., $\frac{\hat{\Phi}(\mathbf{f}_i^*)\big\rfloor_{i=I_{SbD}}}{\hat{\Phi}(\mathbf{f}_i^*)\big\rfloor_{i=1}} \approx 1.65 \times 10^{-7}$ - Fig. 13) and it highlights its effectiveness in handling the additional objectives (i.e., $\hat{\Phi}^{ATT}(\mathbf{f}_i^*)$, and $\hat{\Phi}^{WGT}(\mathbf{f}_i^*)$ - Fig. 13) although some of them naturally exhibit a limited dynamic range (e.g., $\hat{\Phi}^{WGT}(\mathbf{f}_i^*)$ marginally improves as the radome weight is not strongly affected by small variations of the internal radome thickness - Fig. 13).

V. CONCLUSIONS

A high-level review of the SbD paradigm concepts and features has been discussed and its application to the design of complex *EM* systems has been presented. As a representative example, the *SbD*-based design of an electrically-large 3D ogive-shaped radome has been discussed to give some insights on the advantages and the potentialities of the proposed synthesis framework also in comparison with conventional optimization-driven design techniques.

The main outcomes from both the methodological derivation and the numerical validation are (*i*) the *SbD*-based methodology enables the feasible design of complex *EM* structures thanks to the possibility to select the best (i.e., problem-oriented) trade-off functional scheme and the most suitable techniques depending on the available resources and objectives; (*ii*) an accurate selection of the solution descriptors (*DoF*s) is of fundamental importance to mitigate the curse of dimensionality affecting the design of complex systems; (*iii*) the *NFL* theorems [34] hold true for the *SbD* ecosystem, as well, since an improper choice/integration of the functional blocks causes both inefficient design processes and inaccurate designs. Future works within the *SbD* framework will be devoted to further exploit the cross-relationships among the functional blocks of the different "layers" of the design procedure of a complex system as well as to extend the *SbD* application to different scenarios in next generation sensing and communications including the co-design of radomes and phased arrays, as well as the multi-physics optimization of radome material/external descriptors taking into account their mechanical and aerodynamic performance.

ACKNOWLEDGEMENTS

A. Massa wishes to thank E. Vico for her never-ending inspiration, support, guidance, and help.

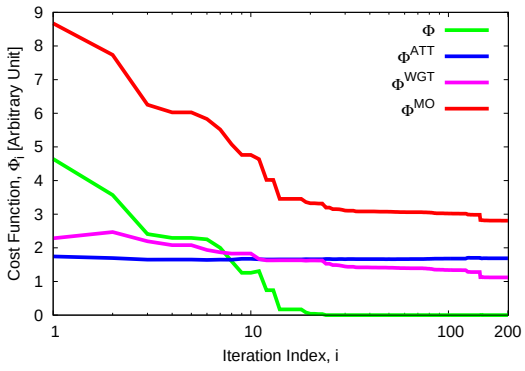

Figure 13. *Numerical Validation* (*Multiple Objective,* $S = 250$) - Evolution of the predicted cost function value, $\hat{\Phi}^{MO}\left(\mathbf{f}_i^*\right)$, and of the three different terms, $\hat{\Phi}\left(\mathbf{f}_i^*\right)$, $\hat{\Phi}^{ATT}\left(\mathbf{f}_i^*\right)$, and $\hat{\Phi}^{WGT}\left(\mathbf{f}_i^*\right)$.

REFERENCES

[1] R. J. Mailloux, *Phased Array Antenna Handbook*, 2nd ed. Norwood, MA, USA: Artech House, 2005.

[2] S. V. Amari and H. Pham, "A novel approach for optimal cost-effective design of complex repairable systems," *IEEE Trans. Syst., Man, Cybern. A, Syst., Humans*, vol. 37, no. 3, pp. 406-415, May 2007.

[3] N. Fourikis, "A parametric study of the constraints related to Gregorian/Cassegrain offset reflectors having negligible cross polarization," *IEEE Trans. Antennas Propag.*, vol. 36, no. 1, pp. 144-147, Jan. 1988.

[4] C. Vegni and F. Bilotti, "Parametric analysis of slot-loaded trapezoidal patch antennas," *IEEE Trans. Antennas Propag.*, vol. 50, no. 9, pp. 1291-1298, Sep. 2002.

[5] R. L. Haupt and D. H. Werner, *Genetic Algorithms in Electromagnetics.* Hoboken, NJ: Wiley, 2007.

[6] P. Rocca, M. Benedetti, M. Donelli, D. Franceschini, and A. Massa, "Evolutionary optimization as applied to inverse scattering problems," *Inverse Probl.*, vol. 25, no. 12, pp. 1-41, Dec. 2009.

[7] P. Rocca, G. Oliveri, and A. Massa, "Differential evolution as applied to electromagnetics," *IEEE Antennas Propag. Mag.*, vol. 53, no. 1, pp. 38-49, Feb. 2011.

[8] F. Hsu, C. Po-Rong, and K.-K. Chan, "Optimization of two-dimensional radome boresight error performance using simulated annealing technique," *IEEE Trans. Antennas Propag.,* vol. 41, no. 9, pp. 1195-1203, Sep. 1993.

[9] P. Rocca, G. Oliveri, R. J. Mailloux, and A. Massa, "Unconventional phased array architectures and design Methodologies - A review," *Proc. IEEE,* vol. 104, no. 3, pp. 544-560, Mar. 2016.

[10] N. Jin and Y. Rahmat-Samii, "Parallel particle swarm optimization and finite- difference time-domain (PSO/FDTD) algorithm for multiband and wide-band patch antenna designs," *IEEE Trans. Antennas Propag.*, vol. 53, no. 11, pp. 3459-3468, Nov. 2005.

[11] R. U. Nair, and R. M. Jha, "Electromagnetic performance analysis of a novel monolithic radome for airborne applications," *IEEE Trans. Antennas Propag.*, vol. 57, no. 11, pp. 3664-3668, Nov. 2009.

[12] B. H. Calhoun, J. Lach, J. Stankovic, D. D. Wentzloff, K. Whitehouse, A. T. Barth, J. K. Brown, Q. Li, S. Oh, N. E. Roberts, and Y. Zhang, "Body sensor networks: a holistic approach from silicon to users," *Proc. IEEE*, vol. 100, no. 1, pp. 91-106, Jan. 2012.

[13] A. Massa, G. Oliveri, P. Rocca, and F. Viani, "System-by-Design: a new paradigm for handling design complexity," *Proc. 8th European Conf. Antennas Propag.*, The Hague, The Netherlands, 2014, pp. 1180-1183.

[14] G. Oliveri, F. Viani, N. Anselmi, and A. Massa, "Synthesis of multi-layer WAIM coatings for planar phased arrays within the system-by-design framework," *IEEE Trans. Antennas Propag.*, vol. 63, no. 6, pp. 2482-2496, Jun. 2015.

[15] G. Oliveri, M. Salucci, N. Anselmi, and A. Massa, "Multiscale System-by-Design synthesis of printed WAIMs for waveguide array enhancement," *IEEE J. Multiscale Multiphys. Comput. Tech.*, vol. 2, pp. 84-96, Jun. 2017.

[16] G. Oliveri, A. Gelmini, A. Polo, N. Anselmi, and A. Massa, "System-by-Design multi-scale synthesis of task-oriented reflectarrays," *IEEE Trans. Antennas Propag.*, vol. 68, no. 4, pp. 2867-2882, Apr. 2020.

[17] J. R. R. A. Martins and A. B. Lambe, "Multidisciplinary design optimization: A survey of architectures," *AIAA Journal*, vol. 51, no. 9, pp. 2049-2075, 2013.

[18] J. Jin, *The Finite Element Method in Electromagnetics*, 2nd. ed. New York, NY: Wiley-IEEE Press, 2002.

[19] E. S. Siah, M. Sasena, J. L. Volakis, P. Y. Papalambros, and R. W. Wiese, "Fast parameter optimization of large-scale electromagnetic objects using DIRECT with Kriging metamodeling," *IEEE Trans. Microwave Theory Tech.*, vol. 52, no. 1, pp. 276-285, Jan. 2004.

[20] M. Salucci, G. Oliveri, N. Anselmi, and A. Massa, "Material-by-design synthesis of conformal miniaturized linear phased arrays," *IEEE Access*, vol. 6, pp. 26367-26382, 2018.

[21] G. M. Sardi, E. Martini, and S. Maci, "Various types of homogenization for metamaterials," *Proc. 7th European Conf. Antennas Propag.* (EuCAP), pp. 3691-3692, 8-12 Apr. 2013.

[22] N. Anselmi, L. Manica, P. Rocca, and A. Massa, "Tolerance analysis of antenna arrays through interval arithmetic," *IEEE Trans. Antennas Propag.*, vol. 61, no. 11, pp. 5496-5507, Nov. 2013.

[23] J. Lee, Y. Lee, and H. Kim, "Decision of error tolerance in array element by the Monte Carlo method," *IEEE Trans. Antennas Propag.*, vol. 53, no. 4, pp. 1325-1331, Apr. 2005.

[24] D.-H. Kwon and D. H. Werner, "Transformation electromagnetics: an overview of the theory and applications," *IEEE Antennas Propag. Mag.*, vol. 52, no. 1, pp. 24-46, Feb. 2010.

[25] M. Salucci, F. Boulos, A. Polo, and G. Oliveri, "Conformal transformation electromagnetics based on Schwarz-Christoffel mapping for the synthesis of doubly-connected metalenses," *IEEE Trans. Antennas Propag.*, vol. 68, no. 3, pp. 1836-1850, Mar. 2020.

[26] S. Jain, M. Abdel-Mageed, and R. Mittra, "Flat-lens design using field transformation and its comparison with those based on transformation optics and ray optics," *IEEE Antennas Wireless Propag. Lett.*, vol. 12, pp. 777-780, 2013.

[27] M. Benedetti, R. Azaro, and A. Massa, "Memory enhanced PSO-based optimization approach for smart antennas control in complex interference scenarios," *IEEE Trans. Antennas Propag.*, vol. 56, no. 7, pp. 1939-1947, Jul. 2008.

[28] W. Xu, B. Y. Duan, P. Li, and Y. Qiu, "A new efficient thickness profile design method for streamlined airborne radomes," *IEEE Trans. Antennas Propag.*, vol. 65, no. 11, pp. 6190-6195, Nov. 2017.

[29] W. Xu, Y. Zong, P. Li, and Y. Qiu, "Variable thickness airborne radome design considering thickness profile control and additional electromagnetic performance," *IEEE Trans. Antennas Propag.*, vol. 69, no. 4, pp. 2443-2448, April 2021.

[30] D. J. Kozakoff, *Analysis of Radome-Enclosed Antennas*, 2nd Ed. Norwood, MA: Artech House, 2010.

[31] J. H. Kim, H. J. Chun, I. C. Hong, Y. J. Kim, and Y. B. Park, "Analysis of FSS radomes based on physical optics method and ray tracing technique," *IEEE Antennas Wireless Propag. Lett.*, vol. 13, pp. 868-871, 2014.

[32] R. U. Nair and R. M. Jha, "Electromagnetic design and performance analysis of airborne radomes: trends and perspectives," *IEEE Antennas Propag. Mag.*, vol. 56, no. 4, pp. 276-298, Aug. 2014.

[33] P. L. Overfelt, "Superspheroids: A new family of radome shapes," *IEEE Trans. Antennas Propag.*, vol. 43, no. 2, pp. 215-220, Feb. 1995.

[34] D. H. Wolpert and W. G. Mcready, "No free lunch theorem for optimization," *IEEE Trans. Evol. Comput.*, vol. 1, no. 1, pp. 67-82, Apr. 1997.

[35] D. Maljovec, B. Wang, A. Kupresanin, G. Johannesson, V. Pascucci, and P. Bremer, "Adaptive sampling with topological scores," *Int. J. Uncertain. Quant.*, vol. 3, no. 2, pp. 119-141, Jan. 2013.